# Analytical and Numerical Study of Joule Heating Effects on Electrokinetically Pumped Continuous Flow PCR Chips

Lin Gui and Carolyn L. Ren*

*Department of Mechanical and Mechatronics Engineering, University of Waterloo, 200 University Ave. West, Waterloo, Ontario, Canada N2L 3G1*

*Received October 15, 2007. In Final Form: December 8, 2007*

Joule heating is an inevitable phenomenon for microfluidic chips involving electrokinetic pumping, and it becomes a more important issue when chips are made of polymeric materials because of their low thermal conductivities. Therefore, it is very important to develop methods for evaluating Joule heating effects in microfluidic chips in a relatively easy manner. To this end, two analytical models have been established and solved using the Green's function for evaluating Joule heating effects on the temperature distribution in a microfluidic-based PCR chip. The first simplified model focuses on the understanding of Joule heating effects by ignoring the influences of the boundary conditions. The second model aims to consider practical experimental conditions. The analytical solutions to the two models are particularly useful in providing guidance for microfluidic chip design and operation prior to expensive chip fabrication and characterization. To validate the analytical solutions, a 3-D numerical model has also been developed and the simultaneous solution to this model allows the temperature distribution in a microfluidic PCR chip to be obtained, which is used to compare with the analytical results. The developed numerical model has been applied for parametric studies of Joule heating effects on the temperature control of microfluidic chips.

## 1. Introduction

Electrokinetic flow has been commonly used as a liquid pumping method in microfluidic devices because of its structure of no moving elements, the degree of flow rate control it allows, and the potential for integration.[1−3] Joule heating is inevitable when electrokinetic pumping is used for microfluidic applications because it requires a high voltage difference applied to the liquid in microchannels. Due to the high surface-to-volume ratio typical of microchannels and high thermal conductivity values that silicon or glass materials have, Joule heating can be reasonably neglected in some applications or reduced through the design of the chip in other applications. However, Joule heating must be carefully considered in the design and control of polymer-made microfluidic chips due to their low thermal conductivity values.[4−5] In the case that Joule heating is utilized as part or the whole heating source such as isoelectric focusing for protein separation in which pH gradients are thermally generated through Joule heating[6−7] and on-chip continuous flow polymerase chain reaction (PCR) in which electrokinetic pumping is used,[8] it is very important to evaluate Joule heating effects for certain designs prior to expensive chip fabrication and characterization processes.[9−10]

In this study, a microfluidic-based continuous flow PCR chip is used as an example to develop models for the evaluation of Joule heating effects, which can be extended to other microfluidic chip applications by slight modifications. PCR is a powerful technique used to exponentially amplify specific target DNA sequences by processing sample mixtures repetitively through a thermal cycle with three designed temperature regions, which are 95 °C for denaturing one double strand DNA template into two single strands, 60 °C for annealing the primers at the two ends of the target sequence, and 75 °C for extending the primers to full sequences.[11−15] Lately, many groups have addressed the need for applying microfluidic chip technology to PCR processes because the high surface-to-volume ratio typical of microchannels leads to lower sample/reagent consumption, higher heat transfer efficiency, and much faster biochemical reaction.[16−18] In a conventional microfluidic PCR chip, sample mixtures are contained in a small chamber, which is programmed to alter its temperature of the reaction every few minutes allowing DNA denaturing and synthesis.[19−20] However, it is difficult to integrate chamber-based microfluidic PCR chip with other processes such as DNA separation and detection using electrophoresis techniques, which is normally designed to occur after PCR processes.

In 1998, Kopp et al.[21] presented a microfluidic PCR chip with a serpentine channel embedded at the center of the chip, which has the potential to be integrated with pre- and post-PCR processes because of its continuous flow nature. In this design, PCR processes are performed by continuously pumping the sample

* Corresponding author. E-mail: c3ren@mecheng1.uwaterloo.ca. Phone: 519-888-4567 x 33030. Fax: 519-885-5862.

(1) Qiao, R. *Langmuir* **2006**, *22*, 7096.
(2) Tian, F.; Li, B.; Kwok, D. Y. *Langmuir* **2005**, *21*, 1126.
(3) Erickson, D.; Li, D. *Langmuir* **2003**, *19*, 5421.
(4) Erickson, D.; Sinton, D.; Li, D. *Lab Chip* **2003**, *3*, 141.
(5) Hu, G. Q.; Xiang, Q.; Fu, R.; Xu, B.; Venditti, R.; Li, D. *Anal. Chim. Acta.* **2006**, *557*, 146.
(6) Kates, B.; Ren, C. L. *Electrophoresis* **2006**, *27*, 1967.
(7) Huang, T.; Pawliszyn, J. *Electrophoresis* **2002**, *23*, 3504.
(8) Chen, J. F.; Wabuyele, M.; Chen, H. W.; Patterson, D.; Hupert, M.; Shadpour, H.; Nikitopoulos, D.; Soper, S. A. *Anal. Chem.* **2005**, *77*, 658.
(9) Tang, G. Y.; Yang, C.; Chai, C. J.; Gong, H. Q. *Langmuir* **2003**, *19*, 10975.
(10) Kang, Y.; Yang, C.; Huang, X. *Langmuir* **2005**, *21*, 7598.
(11) Chang, H. C.; Leaw, S. N.; Huang, A. H.; Wu, T. L.; Chang, T. C. *J. Clin. Microbiol.* **2001**, *39*, 3466.
(12) Gillespie, S. H.; Ullman, C.; Smith, M. D.; Emery, V. *J. Clin. Microbiol.* **1994**, *32*, 1308.
(13) Dieffenbach, C. W.; Dveksler, G. S. *PCR Primer: A Laboratory Manual*, 2nd ed.; Cold Spring Harbor Lab Press: New York, 2003; Chapter 1.
(14) Mai, M.; Grabs, R.; Barnes, R. D.; Vafiadis, P.; Polychronakos, C. *BioTechniques* **1998**, *25*, 208.
(15) Markoulatos, P.; Siafakas, N.; Katsorchis, T.; Moncany, M. *J. Clin. Labor. Anal.* **2003**, *17*, 108.
(16) Liu, D. Y.; Zhou, X. M.; Zhong, R. T.; Ye, N. N.; Chang, G. H.; Xiong, W.; Mei, X. D.; Lin, B. C. *Talanta* **2006**, *68*, 616.
(17) Prakash, A. R.; Adamia, S.; Sieben, V.; Pilarski, P.; Pilarski, L. M.; Backhouse, C. J. *Sens. Actuators B* **2006**, *113*, 398.
(18) Auroux, P. A.; Koc, Y.; Mello, A.; Manz, A.; Day, P. J. R. *Lab Chip* **2004**, *4*, 534.
(19) Legendre, L. A.; Bienvenue, J. M.; Roper, M. G.; Ferrance, J. P.; Landers, J. P. *Anal. Chem.* **2006**, *78*, 1444.
(20) Daniel, J. H.; Iqbal, S.; Millington, R. B.; Moore, D. F.; Lowe, C. R.; Leslie, D. L.; Lee, M. A.; Pearce, M. J. *Sens. Actuators A* **1998**, *71*, 81.
(21) Kopp, M. U.; Mello, A. J.; Manz, A. *Science* **1998**, *280*, 1046.

10.1021/la703201p CCC: $40.75 
Published on Web 02/08/2008

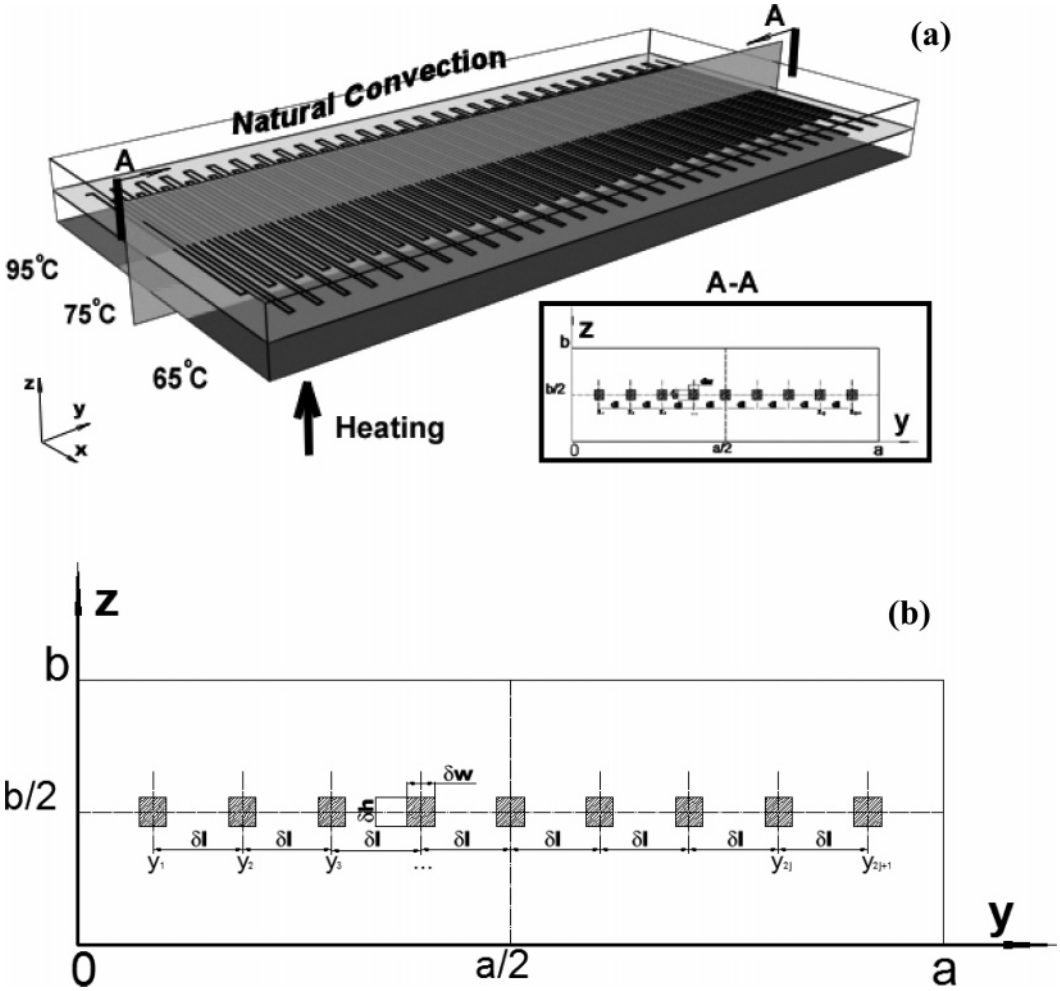


**Figure 1.** (a) Sketch of a normal continuous flow PCR chip and (b) sketch of the 2D mathematical model.

mixtures through a long serpentine channel, beneath which are three thermostated copper blocks providing the three required temperatures (i.e., 95, 60, and 75 °C), respectively. Because of its low processing time and potential for integration with other operations, continuous flow PCR chips have been subject to an extensive worldwide study since it was first reported by Kopp et al.[22−28] In Kopp's design, pressure-driven flow was employed to pump sample mixtures through microchannels. In order to integrate pressure-pumped microfluidic chips with other processes, multiple on-chip valves and connectors are required to achieve operational control, which is very difficult to implement. Another alternate is electrokinetic pumping, which has many advantages over pressure-driven pumping for on-chip DNA analysis such as high resolution of separation and ease of integration. However, when electrokinetic flow or a combination of electrokinetic and pressure driven flow is used as a pumping method for a continuous flow microfluidic PCR chip, significant Joule heating will be generated. Joule heating effect will become even noticeable for a chip with a large number of microchannels and made of polymeric materials such as polydimethylsiloxane (PDMS).[4−5] Therefore, it is very necessary to develop an analytical tool for evaluating Joule heating effects for electrokinetic-pumped microfluidic PCR chips, which is also the main goal of this work.

There have been many studies reported recently about Joule heating effects on electrokinetic flow in microchannels.[4,29−33] Erickson et al.[4] numerically and experimentally examined Joule heating effects on the temperature distribution in a T-shaped microchannel. In their study, significant temperature gradients were observed at the intersection, especially for a PDMS chip. Tang et al.[29] reported a 3-D numerical model studying Joule heating effects on electrokinetic transport in microchannels. Their model predicted that the conventional plug-like electroosmotic velocity profile was distorted when Joule heating was considered, which reasonably agreed with their experimental studies. A similar distorted electroosmotic velocity profile was also observed by Xuan et al.[30] in their experiments, in which a caged-fluorescent dye was used to measure the velocity profile. The influence of Joule heating on separation efficiency in capillary electrochromatography was observed by Chen et al.[31] Their study indicated that separation efficiency decreases due to the presence of Joule

(22) Hashimoto, M.; Chen, P. C.; Mitchell, M. W.; Nikitopoulos, D. E.; Soper, S. A.; Murphy, M. C. *Lab Chip* **2004**, *4*, 638.
(23) Chen, Z. Y.; Qian, S. Z.; Abrams, W. R.; Malamud, D.; Bau, H. H. *Anal. Chem.* **2004**, *76*, 3707.
(24) Nakano, H.; Matsuda, K.; Yohda, M.; Nagamune, T.; Endo, I.; Yamane, T. *Biosci, Biotechnol. Biochem.* **1994**, *58*, 349.
(25) Liu, J.; Enzelberger, M.; Quake, S. *Electrophoresis* **2002**, *23*, 1531.
(26) Bu, M. Q.; Melvin, T.; Ensell, G.; Wilkinson, J. S.; Evans, A. G. R. *J. Micromech. Microeng.* **2003**, *13*, S125.
(27) Wang, W.; Li, Z. X.; Luo, R.; Lv, S. H.; Xu, A. D.; Yang, Y. J. *J. Micromech. Microeng.* **2005**, *15*, 1369.
(28) Gui, L.; Ren, C. L. *Anal. Chem.* **2006**, *78*, 6215.
(29) Tang, G. Y.; Yan, D. G.; Yang, C.; Gong, H.; Chai, J. C.; Lam, Y. C. *Electrophoresis* **2006**, *27*, 628.
(30) Xuan, X. C.; Xu, B.; Sinton, D.; Li, D. *Lab Chip* **2004**, *4*, 230.
(31) Chen, G. F.; Tallarek, U.; Seidel-Morgenstern, A.; Zhang, Y. K. *J. Chromatogr. A* **2004**, *1044*, 287.
(32) Chein, R. Y.; Yang, Y. C.; Lin, Y. S. *Electrophoresis* **2006**, *27*, 640.
(33) West, J.; Hurley, E.; Cordero, N.; Collins, J. K.; Lane, W.; Berney, H. *Anal. Chim. Acta.* **2004**, *527*, 1.

heating which results in the increased axial diffusion of the analyte molecules and the nonuniform electroosmotic velocity profile as found by others. To date, there are a limited number of studies about Joule heating effects on continuous flow PCR applications. Hu et al. recently presented a numerical model to determine the parameters required to achieve desired thermal cycling, which was also validated through their PCR experiments for the amplification of *E. coli* O157:H7 strain.[5] In their study, only a simple case of one straight microchannel was considered; however, most PCR chips have a network of microchannels, which require a more complicated model to evaluate Joule heating effects.

More importantly, when numerical simulation is not feasible or expensive for many applications, analytical models are very useful for the estimation of Joule heating effects. Therefore, in this study, two analytical models were developed and presented to examine the influences of Joule heating on heat transfer in an electrosomosis-based continuous flow PCR chip with different boundary conditions, which aim to simulate two sets of commonly encountered experimental conditions. A numerical model was also developed to validate the analytical models. Parametric studies of Joule heating effects on the temperature distribution of the chip were performed based on the simultaneous solution of the numerical model.

## 2. Theoretical Analysis

Figure 1a shows the sketch of a continuous flow PCR chip, in which a long serpentine microchannel is embedded at the center along the chip thickness direction. For model simplification, the chip is assumed to consist of three layers, the top substrate, the middle layer with microchannels, and the bottom substrate. Heaters are assumed to be placed beneath the bottom substrate to keep the three designed temperature regions as required for PCR processes.

For many microfluidic chip applications, the fluid temperature is often measured by mixing a temperature-dependent fluorescent dye with the sample.[34] However, it is difficult to conduct real-time temperature measurements and make corresponding control on temperatures through the heaters. Therefore, for PCR applications, the fluid temperature in microchannels can be evaluated and controlled according to the temperature of the substrate, which can be kept stable by heaters beneath the substrate and can be experimentally measured and controlled. To this end, accurate prediction of temperature difference between the fluid in the microchannel and the bottom substrate is key. The models developed and presented here allow the temperature distribution in the chip thickness direction to be obtained, which can predict this temperature difference and thus the temperature distribution in a chip.

**2.1. Mathematical Model with Homogeneous Boundary Conditions.** In order to provide a clear overview of the effects of Joule heating and channel locations on the temperature distribution in a microfluidic chip, which is particularly important when designing a polymer-made, electrokinetically pumped PCR chip, a simplified mathematical model was first developed. In this model, homogeneous boundary conditions were chosen aiming to ignore the influences of the boundary conditions and a steady-state condition was considered. This model allows the temperature distribution on the middle plane (the A−A plane in Figure 1a) along the chip width direction ($x$ direction) to be determined, in which the temperature distribution in the channel can be determined if the temperature of the substrate is known. The detailed sketch of the domain of interest is shown in Figure 1b. There are a specific number (i.e., $2j + 1$) of rectangular channels passing through this plane, where $j$ represents the number of the microchannel completely passing through the half of the chip length (i.e., $a/2$).

For simplicity, the steady state was considered first to make it clear how the main parameters, such as Joule heating and channel/chip dimensions, contribute to the final temperature distribution. The homogeneous boundary conditions used were $\partial T/\partial y = 0$ @ $y = 0$, $\partial T/\partial y = 0$ @ $y = a$, $\partial T/\partial y = 0$ @ $z = b$ (no heat flux exists on the boundaries), and $T = 0$ @ $z = 0$ (constant zero temperature on the boundary $z = 0$) where $a$ is the chip length and $b$ the chip thickness. Assuming uniform thermal properties through the entire chip, the governing equation for this model is

$$\frac{\partial^2 T}{\partial y^2} + \frac{\partial^2 T}{\partial z^2} + \frac{1}{k} g(y,z) = 0 \tag{1}$$

where $k$ is the thermal conductivity of the medium, $g$ is the heat source term which is equal to $q$ in the liquid region accounting for Joule heating generated in the microchannel or zero for the substrates in the other areas, such as

$$g(y,z) = \begin{cases} q & y_i - \dfrac{\delta w}{2} \le y \le y_i + \dfrac{\delta w}{2}, \dfrac{b}{2} - \dfrac{\delta h}{2} \le z \le \dfrac{b}{2} + \dfrac{\delta}{2} \\ 0 & \text{else} \end{cases}$$

where $i = 1, 2, ..., 2j + 1$, $y_i = a/2 - j\delta l + (i - 1)\delta l$, $\delta w$ is the microchannel width, $\delta h$ is the microchannel depth, and $\delta l$ is the horizontal distance between two adjacent microchannels measured from center to center. The Joule heating source, $q$, can be evaluated by $q = \sigma \vec{E}\vec{E}$ where $\sigma$ is the electrical conductivity of the PCR reaction mixture which can be experimentally measured, and $\vec{E}$ is the electrical field strength. The temperature dependence of $\sigma$ is not considered here for the analytical solution to be possible. The analytical solution to eq 1 was obtained using the Green's function method:[35]

$$T(y,z) = \frac{4\sqrt{2}q}{kab}\left\{\sum_{n=1}^{\infty} \frac{2j+1}{{\gamma_n}^3} \delta w \sin\frac{\gamma_n b}{2} \times \sin\frac{\gamma_n \delta h}{2} \sin(\gamma_n z) + \sum_{m=1}^{\infty}\sum_{n=1}^{\infty} \frac{4G_1}{({\beta_m}^2 + {\gamma_n}^2)\beta_m \gamma_n} \times (1 + 2\sum_{i=1}^{j} \cos(i\beta_m \delta l)) \cos(\beta_m y) \sin(\gamma_n z)\right\} \tag{2}$$

where, $G_1 = \sin(\gamma_n b/2) \cos(\beta_m a/2) \sin(\beta_m \delta w/2) \sin(\gamma_n \delta h/2)$, $\gamma_n = \pi(2n - 1)/2b$ $\beta_m = m\pi/a$, $m = 0, 1, 2, ...$ and $n = 1, 2, 3, ....$ The solution shown in eq 2 was simplified by considering that $\cos(\beta_m a/2) = 0$ when $m = 2l + 1 (l = 1, 2, 3, ...)$. Let $m = 2l (l = 1, 2, 3, ...)$ and substitute it into the solution, eq 2

(34) Xiang, Q.; Xu, B.; Fu, R.; Li, D. *Biomed. Microdevices* **2005**, *7*, 273.

(35) Ozisik, M. N. *Heat conduction*, 1st ed.; John Wiley & Sons: New York, 1980.

$$T(y,z) = \frac{4\sqrt{2}q}{kab}\left\{\sum_{n=1}^{\infty}\frac{2j+1}{{\gamma_n}^3}\delta w \sin\frac{\gamma_n b}{2}\sin\frac{\gamma_n \delta\, h}{2}\times \sin(\gamma_n z) + \sum_{l=1}^{\infty}\sum_{n=1}^{\infty}\frac{4G_2}{({\beta_{2l}}^2+{\gamma_n}^2)\beta_{2l}\gamma_n}\times (1+2\sum_{i=1}^{j}\cos(i\beta_{2l}\,\delta l))\cos(\beta_{2l}y)\sin(\gamma_n z)\right\} \quad (3)$$

where $G_2 = \sin(\gamma_n b/2)\cos(\beta_{2l}a/2)\sin(\beta_{2l}\delta\ w/2)\sin(\gamma_n \delta\ h/2)$. Equation 3 was further simplified considering that when $l$ and $n$ increase, only the first largest term in the series is dominate (i.e., the terms with $l = 1$ and $n = 1$) and the fact that $\delta\ w \ll a$, $\delta\ h \ll b$, and $b \ll a$. The simplified solution was

$$T(y,z) \approx \frac{4\sqrt{2}bq\ \delta w\ \delta h(2j+1)}{ak\pi^2}\times \sin\frac{\pi}{2b}z\left(1-2\frac{2\sum_{i=1}^{j}\cos(2i\pi\delta\ l/a)+1}{2j+1}\cos\frac{2\pi}{a}y\right) \quad (4)$$

As shown in eq 4, the temperature is directly proportional to the term, $q\ \delta w\ \delta h\ (2j+1)$, which is the total Joule heating generated by the $2j+1$ number of channels. The temperature is also directly proportional to the aspect ratio of the chip, $b/a$, which depicts how thick the chip is. Because heat can be dissipated more easily with a thinner substrate (i.e., $b$ is small), the Joule heating effects will be reduced for a thinner chip.

**2.2. Mathematical Model with More Practical Boundary Conditions.** Although eq 4 provides a clear view of how Joule heating contributes to the steady-state temperature distribution in the chip, the homogeneous boundary conditions used in this model are not practically true. Another transient analytical model was therefore developed aiming for considering real experimental conditions. In detail, the entire chip was assumed to be the same temperature at the beginning (i.e., $T = T_0$ @ $t = 0$, where $T_0$ is room-temperature). During the process, the temperature at the bottom was assumed to be constant ($T = T_1$ @ $z = 0$). Natural convection condition which is true for most experiments was considered at the top of the chip ($-k\partial T/\partial z = h_w(T - T_f)$@ $z = b$, where $h_w$ is the heat transfer coefficient of natural convection). Because the chip thickness is much smaller than the length (i.e., $b \ll a$), natural convection at the side walls was neglected, compared with that on the top. Under this assumption, adiabatic boundary condition was adopted at the two sides of the chip, such as $\partial T/\partial y = 0$ @ $y = 0$ and $\partial T/\partial y = 0$ @ $y = a$. For simplification of the analytical model, uniform thermal properties were assumed in the entire region. Based on the above discussion, the governing equation describing the temperature distribution in the chip takes the format of

$$\frac{\partial^2 T}{\partial y^2} + \frac{\partial^2 T}{\partial z^2} + \frac{1}{k}g(y,z) = \frac{1}{\alpha}\frac{\partial T}{\partial t} \quad (5)$$

where $\alpha$ is the thermal diffusivity of the medium including both the liquid and solid materials. The analytical solution to the above model (eq 5 and its boundary conditions) was obtained using the Green's function method[35] such as

$$T(y,z,t) = T_0 + \frac{4q(2j+1)\delta w}{ak}\sum_{n=1}^{\infty}G_3(1-e^{-\alpha\gamma_n^2 t})\sin\frac{\gamma_n b}{2}\times \sin\frac{\gamma_n \delta h}{2}\sin(\gamma_n y) + \frac{16q}{ak}\sum_{m=1}^{\infty}\sum_{n=1}^{\infty}G_4(1-e^{-\alpha(\beta_m^2+\gamma_n^2)t})\times \sin\frac{\gamma_n b}{2}\sin\frac{\gamma_n \delta h}{2}\sin\frac{\beta_m \delta w}{2}\left(\sum_{l=1}^{2j+1}\cos(\beta_m y_l)\right)\cos(\beta_m y)\times \sin(\gamma_n z) + \frac{2h_w(T_f - T_0)}{k}\sum_{n=1}^{\infty}G_5(1-e^{-\alpha\gamma_n^2 t})\sin(\gamma_n b)\times \sin(\gamma_n z) + 2(T_1 - T_0)\sum_{n=1}^{\infty}G_6(1-e^{-\alpha\lambda_n t})\sin(\gamma_n z) \quad (6)$$

where $G_3 = (k^2\gamma_n^2 + h_w^2)/(\gamma_n^3[b(k^2{\gamma_n}^2 + h_w^2) + kh_w])$, $G_4 = (k^2\gamma_n^2 + h_w^2)/((\beta_m^2 + \gamma_n^2)\beta_m\gamma_n[b(k^2\gamma_n^2 + h_w^2) + kh_w])$, $G_5 = (k^2\gamma_n^2 + h_w^2)/(\gamma_n^2[b(k^2\gamma_n^2 + h_w^2) + kh_w])$, $G_6 = (k^2\gamma_n^2 + h_w^2)/(\gamma_n[b(k^2\gamma_n^2 + h_w^2) + kh_w])$, $\beta_m = m\pi/a$ with $m = 1, 2, 3, \ldots$ and $\gamma_n$ is the solution of the equation, $k\gamma_n \cot(\gamma_n b) + h_w = 0$ with $n = 1, 2, 3, \ldots$.

Equation 6 is the temperature distribution predicted by the analytical model and consists of five terms on the right-hand side illustrating the effects of the experimental system and conditions on the temperature distribution. Briefly, the first term on the right-hand side is the initial temperature, the second term shows the effect of Joule heating, the third term reveals the effect of the channel location, the fourth term accounts for the influences of the natural convection condition and the fifth term shows the effect of heating at the bottom. Although the expression of the solution looks complicated, it is much easier to calculate for a given system than performing numerical simulations, which normally require expensive computing. Therefore, it is very beneficial to studies where numerical simulation is not available or too expensive.

What should be pointed out here is that this solution does not converge to the boundary conditions at $z = b$ and $z = 0$. In other words, the solution, eq 6, cannot accurately predict the temperatures at these two boundaries. This is because the terms associated with the boundary conditions (i.e., the fourth and fifth terms on the right-hand of eq 6) are in the form of the Fourier series that are not uniformly convergent at the boundaries, $z = 0$ and $z = b$. In order to find the solution at these two locations, the equivalent closed-form expressions of eq 6 must be found. To seek the equivalent closed-form expressions, the following 1-D (in the thickness direction) steady-state heat transfer problem was considered, which has the same boundary conditions as above ($T = T_1$ @ $z = 0$ and $-k\ \mathrm{d}T/\mathrm{d}z = h_w(T - T_f)$@ $z = b$). This problem can be described by

$$\frac{\mathrm{d}^2 T}{\mathrm{d}z^2} = 0 \qquad 0 < z < b \quad (7)$$

The solution to this problem can be easily obtained as

$$T(z) = T_1 + \frac{h_w(T_f - T_1)}{k + h_w b}z \quad (8)$$

It should be noted that the above problem is a special case of that described by eq 5 with the extreme conditions that $t \to \infty$ (steady state), $a \to \infty$ (one dimension), and $q = 0$ (no heat source). Therefore, the solution to eq 5 (i.e., eq 6), should be equivalent to eq 8 under these conditions. Substituting $t \to \infty$, $a \to \infty$, and $q = 0$ into eq 6 yields

$$T(z) = T_0 + \frac{2h_w(T_f - T_0)}{k}\sum_{n=1}^{\infty} G_3 \sin(\gamma_n b)\sin(\gamma_n z) + 2(T_1 - T_0)\sum_{n=1}^{\infty} G_4 \sin(\gamma_n z) \quad (9)$$

As discussed above, eq 9 is equivalent to eq 8, which yields

$$T_1 + \frac{h_w(T_f - T_1)}{k + h_w b} z = T_0 + \frac{2h_w(T_f - T_0)}{k}\sum_{n=1}^{\infty} G_3 \sin(\gamma_n b)\sin(\gamma_n z) + 2(T_1 - T_0)\sum_{n=1}^{\infty} G_4 \sin(\gamma_n z) \quad (10)$$

Substituting eq 10 into eq 6 to replace part of the last two terms on the right-hand of eq 6, which are not uniformly convergent at the boundaries, the solution becomes

$$T(y,z,t) = T_1 \frac{h_w(T_f - T_1)}{k + h_w b} z + \frac{4q(2j+1)\delta w}{ak}\sum_{n=1}^{\infty} G_1(1 - e^{-\alpha\gamma_n^2 t})\sin\frac{\gamma_n b}{2}\sin\frac{\gamma_n \delta h}{2}\sin(\gamma_n z) + \frac{16q}{ak}\sum_{m=1}^{\infty}\sum_{n=1}^{\infty} G_2(1 - e^{-\alpha(\beta_m^2 + \gamma_n^2)t})\sin\frac{\gamma_n b}{2} \times \sin\frac{\gamma_n \delta h}{2}\sin\frac{\beta_m \delta w}{2}\left(\sum_{l=1}^{2j+1}\cos(\beta_m y_l)\right)\cos(\beta_m y)\sin(\gamma_n z) - \frac{2h_w(T_f - T_0)}{k}\sum_{n=1}^{\infty} G_3 e^{-\alpha\gamma_n^2 t}\sin(\gamma_n b)\sin(\gamma_n z) - 2(T_1 - T_0)\sum_{n=1}^{\infty} G_4 e^{-\alpha\lambda_n^2 t}\sin(\gamma_n z) \quad (11)$$

Equation 11 is the analytical solution of the temperature at the boundaries: $z = 0$ and $z = b$, which has the similar format to eq 6. Thus eqs 6 and 11 provide the complete solution to the problem identified by eq 5.

Figure 2 shows the analytically predicted temperature distribution in the chip at steady state where eq 6 was used for predicting the temperature in the entire domain except the area near the boundaries (near the boundaries, the eq 6 converges very slowly due to the reason mentioned above, while eq 11 is much faster and better to predict the temperature) and eq 11 was used for predicting the temperature near the boundary locations (i.e., $z = 0$ and $z = b$). In this case, only three channels with a cross-sectional area of 200 $\mu$m × 50 $\mu$m were considered (i.e., $j = 1$). In this figure, PDMS were assumed to be the channel material and the thermal properties of PDMS used in the study are listed in Table 1. The electric field intensity in the microchannel was 10 kV/m. As shown in Figure 2, the effect of Joule heating is appreciable. Because the thermal conductivity of PDMS is relatively low and Joule heating cannot be dissipated quickly, the temperature in the vicinity of the microchannel is much higher (i.e., peaks shown in Figure 2a) than that of the surrounding area. Compared with the width of the channel (200 $\mu$m), the distance between channels is fairly large in this case (1.25 cm); therefore, the channels hardly affect each other. This result will be validated by the numerical results given later.

## 3. Numerical Model

**3.1. Model Description.** To validate the above analytical models, a 3D numerical model was developed and the simulations

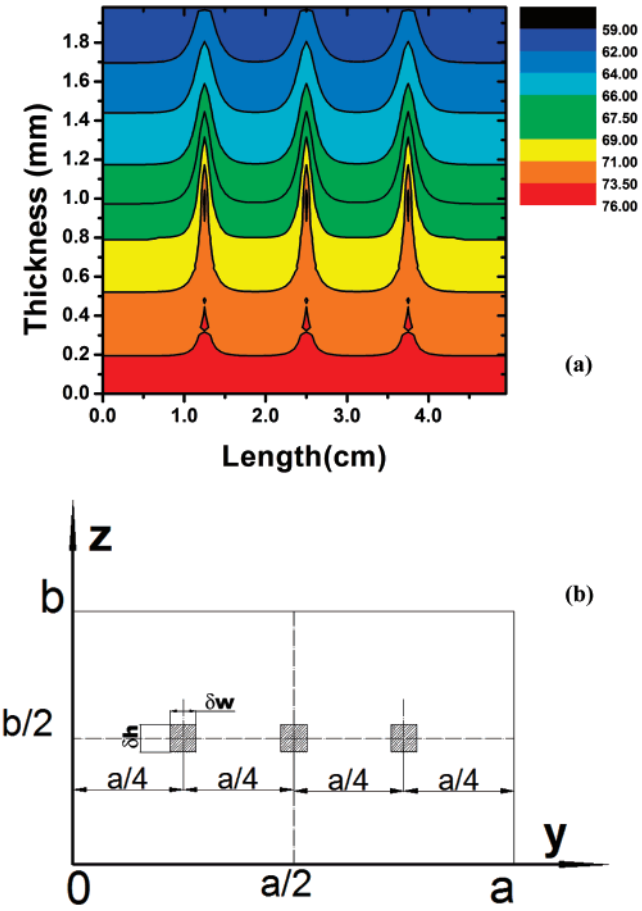


**Figure 2.** Analytical result of temperature distribution when $j = 1$ and $t = 10\,000$ s.

**Table 1. Typical Thermal Properties of PDMS**

| properties | $\lambda$ (W/m·K) | $\rho$ (kg/m$^3$) | $c$ (J/kg·°$C$) |
|---|---|---|---|
| PDMS | $1.5 \times 10^{-1}$ | $0.97 \times 10^3$ | $1.46 \times 10^3$ |

were performed as follows to draw a brief picture of a more practical model. Figure 3 shows the sketch of the computational domain and grids used in the simulation. The chip is assumed to consist of two layers with the same thicknesses, but different materials. In the simulations, two commonly used materials were considered: PDMS and glass. The microchannel is located in one of the substrates and the subfigure in Figure 3 shows the layout of the microchannel viewed from the top. For clarity, only one cycle is drawn in Figure 3 and each cycle includes three regions: a high-temperature region, (denaturation), a low-temperature region (annealing), and a medium-temperature region (extension). Because of the design of continuous flow, the fluid in the channel does not flow directly from the high-temperature region to the low-temperature region as required in PCR processes; instead, it must pass the medium-temperature region, which is unnecessary in the conventional PCR amplification method. To eliminate the effect of this unnecessary segment as much as possible, each region is designed short and the channel is required to be bended several times in each reaction region allowing sufficient time for reaction. The channel length ratio for three regions ($n_1$:$n_2$:$n_3$ for denaturation : annealing : extension) can be changed as one likes in the model to meet different demands of time ratio. Figure 4 shows a one-cycle layout which has a ratio of $n_1$:$n_2$:$n_3$ = 2:2:8, which gives a time ratio of 1:1:4 for three reaction periods. In the practical simulations, a typical three-cycle layout was considered which includes the first cycle, a medium cycle and the final cycle.

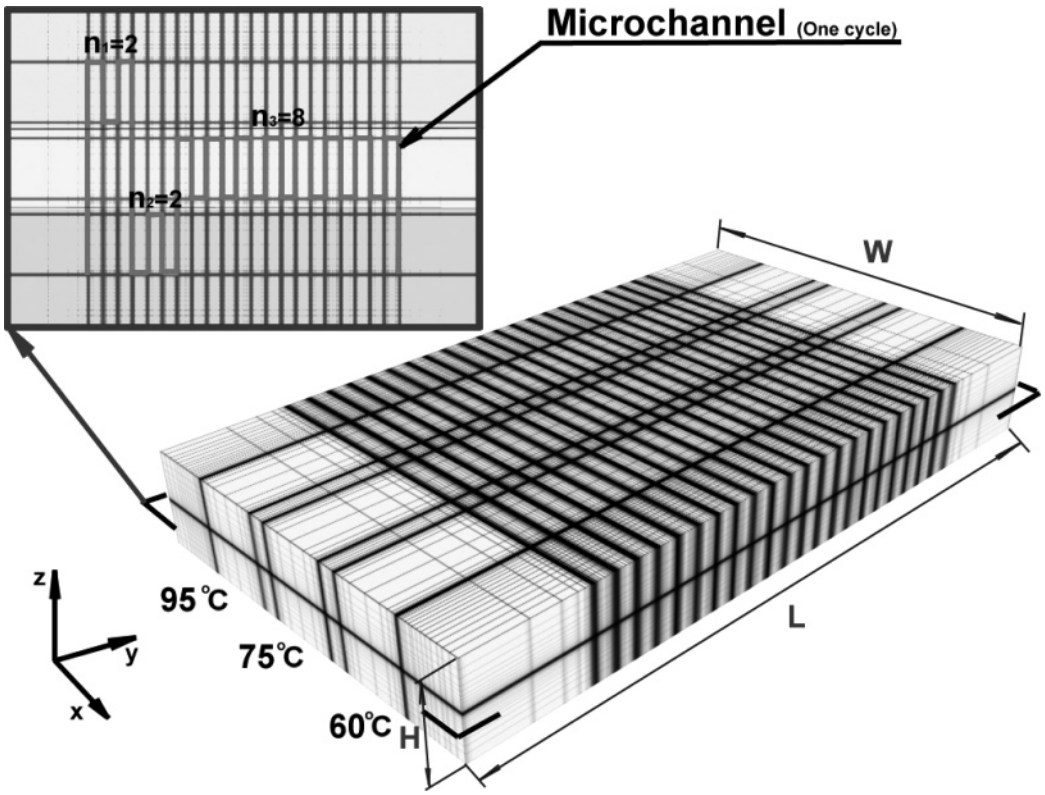


**Figure 3.** Sketch of the computational domain and grids used in the numerical model.

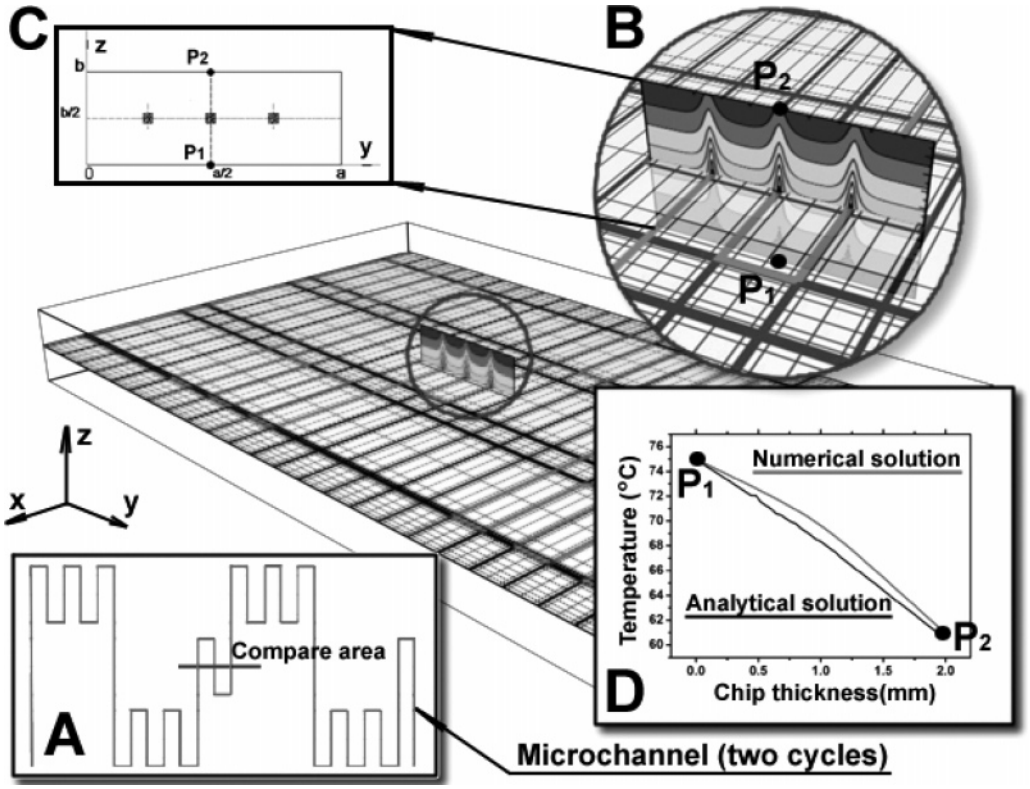


**Figure 4.** Comparison of numerical and analytical solutions.

**3.2. Governing Equations.** During the simulation, all of the fluid and substrates were considered as one material with variable thermal properties. For electrokinetic flow, the flow velocity is usually very small (for example, fluid velocity is only 0.45 mm/s for a mM buffer solution under an electrical field strength of 10 kV/m). Therefore, the energy transfer caused by the convection in the channel is negligible compared with the strong heat transfer from bottom to top. For this reason, the flow field was not considered in the following simulations. This reasonable simplification greatly saved the computational time and had been successfully applied previously.[26,36] Because PCR processes often

(36) Yang, W. P.; Du, L. Q.; Wang, J.; Ma, L. Z.; Zhu, J. B. *Sens. Actuators B* **2005**, *108*, 695.

begin after the thermal field of the whole PCR chip reaches steady state, the characteristic length is still the width of the microchannel. Thus, the nondimensional governing equation can be given as follows:

$$\bar{\rho}C_p \frac{\partial \Theta}{\partial \tau} = \vec{\nabla}(\Lambda \cdot \vec{\nabla}\Theta) + \dot{\mathscr{Q}} \quad (12)$$

where $\bar{\rho}$ is the nondimensional density ($\bar{\rho} = \rho/\rho_0$ where $\rho_0$ is the density of the solution), $C_p$ is the nondimensional heat capacity ($C_p = c/c_0$ where $c_0$ is the heat capacity of the solution), $\Lambda$ is the nondimensional heat conductivity ($\Lambda = \lambda/\lambda_0$ where $\lambda_0$ is the heat conductivity of the solution), $\Theta$ is the nondimensional temperature ($\Theta = (T - T_{low})/T_{high} - T_{low}$) where $T_{high} = 95\ ^\circ C$ taken to be the temperature of denaturation, and $T_{low} = 65\ ^\circ C$ the temperature of annealing), $\dot{\mathscr{Q}}$ is the nondimensional heat source ($\dot{\mathscr{Q}} = \dot{q}l^2/\lambda_0(T_{high} - T_{low})$ where $q = \sigma\vec{E}\vec{E}$ is the Joule heating where the temperature-dependent electrical conductivity can be evaluated by $\sigma = 0.84[1 + 0.03(T - T_0)]$[33] and $T_0$ denotes room-temperature (i.e., 25 °C here), $\tau$ is the nondimensional time ($\tau = t/t_1$, where $t_1 = l^2/\alpha_0$ is the characteristic time of heat transfer in microchannels). In general the characteristic time $t_1$ is very small (i.e., 0.015 s) when considering that the characteristic length $l$ is 50 $\mu$m and $\alpha_0 = 16.9 \times 10^{-8}$ m$^2$/s. That is to say that the thermal field will attain steady state within 20 ms, which is much smaller as compared to PCR processes. Therefore, it is reasonable to ignore the transient item in eq 12

$$\vec{\nabla}(\Lambda \cdot \vec{\nabla}\Theta) + \dot{\mathscr{Q}} = 0 \quad (13)$$

The temperature distribution at the bottom surface is kept constant according to the requirements for three temperature regions (95, 60, and 75 °C). Placed in the environment of room-temperature, the natural convection boundary condition is considered at the top surface of the chip ($(\lambda_0/l)\Lambda\partial\Theta/\partial z|_{top} = \hbar_\infty(\Theta_{wall} - \Theta_0)$) where $\Theta_0$ is the nondimensional room-temperature ($\Theta_0 = (T_0 - T_{low})/(T_{high} - T_{low})$), and $\Theta_{wall}$ is the nondimensional temperature at the top surface and $\hbar_\infty$ is the heat transfer coefficient of natural convection given by $\hbar_\infty = Nu\lambda_{air}/L$, where, $\lambda_{air}$ is the heat conductivity of air, $L$ is the chip length, and $Nu = 0.62(Gr \cdot Pr)^{0.25}$ is the Nussel number of natural convection chosen from,[37] where, $Gr$ is the Grashof number ($Gr = g\beta\Delta TL^3/\upsilon_{air}^2$, where $g$ is the gravitational acceleration, $\beta$ is the thermal expansion coefficient which for gases is $1/T$, $\Delta T$ is the temperature difference between the wall and ambient air, $\upsilon_{air}$ is the kinematic viscosity of air), and $Pr$ is the Prandtl number of air. Considering that the chip thickness is very small, natural convection at the side walls can be neglected compared to that at the top surface. Therefore, adiabatic boundary condition is adopted in the simulation at all the side walls.

**3.3. Numerical Algorithm.** The 3D model was solved using a specially developed program written in C++ based on the finite difference method. The dimension of channel is very small compared with that of the chip; therefore, nonuniform grids were used with fine grids in the channel region to capture changes within the channel dimension. The step of fine grids transited gradually to that of the adjacent coarse grids by a fixed factor which was automatically calculated in the simulation.

**3.4. Validation of the Analytical Model.** To validate the analytical model, the parameters, such as the chip size and layout, in the numerical model were carefully chosen to be comparable to the analytical solution given by Figure 2 (using eq 6). The comparison between the numerical result and the analytical result is given in Figure 4 for a two-cycle layout with a ratio of $n_1$:$n_2$:$n_3$ = 3:3:1. The reason for choosing this ration is to make the calculation area of the two models as close as possible. Figure 4A illustrates the geometry of the entire channel viewed from top and Figure 4B shows the temperature distribution at the middle vertical plane (the dark line in Figure 4A shows its projection on x-y plane). One can find that the numerically predicted temperature distribution is very similar to that shown in Figure 2. Considering that the width of the chip is much larger than the thickness, one can neglect the heat transfer along the width direction (the $x$ direction). Thus the 3D problem can be simplified to a 2D problem. For the same reason, the heat transfer at the side boundary can also be neglected reasonably, which leads to adiabatic boundary conditions. After these simplifications, the temperature distribution in the plane should be exactly same as the temperature distribution given by Figure 2. Figure 4C shows the sketch of the model used for this comparison and Figure 4D shows the temperature distribution along the $P_1P_2$ line (the middle vertical line of the plane) obtained from the numerical and analytical models at $\tau$ = 10000 s. As shown in Figure 4D, reasonable agreements were observed, which validated the present numerical model to a certain extent.

The discrepancy between these two models can be explained as follows. First, the analytical solution was given at $\tau$ = 10000 s; however, the numerical solution is a steady-state solution. Although 10000 s is a fairly long time for thermal equilibrium, the temperature field given by the analytical solution tends to increase after 10000 s, which will decrease the discrepancy between these two solutions. Second, neglecting the heat transfer along the width direction can also bring errors. In fact, in the numerical simulation, the high-temperature region (95 °C) tends to increase the temperature in the middle, while the low-temperature region (60 °C) tends to decrease it. With the same distance, the temperature difference on the high-temperature region side (95 °C − 75 °C = 20 °C) is larger than that on the low-temperature region side (75 °C − 60 °C = 15 °C), which means that the high-temperature region (i.e., 95 °C) will affect the temperature on the calculation plane more than the low-temperature region. Therefore, the numerical result should be a little higher than the analytical result as shown in Figure 4D.

## 4. Results and Discussions

Parametric studies were also performed using the numerical model. Without losing generality, most physical and thermal properties of the liquid were chosen from that of pure water considering the concentration of most commonly used buffer solutions in PCR applications is on the order of mM. Two kinds of ordinary solid materials, glass and PDMS, were considered for PCR chip materials. The detailed running parameters used here are listed in Table 1.[38] All the simulations were based on a three-cycle layout with a ratio of $n_1$:$n_2$:$n_3$ = 2:2:8.

**4.1. Effect of Channel Cross-Sectional Area.** Figure 5 shows the temperature distributions at the middle plane of a hybrid PDMS/glass chip with a channel cross section of 50 $\mu$m × 50 $\mu$m. Figure 5a shows the temperature distribution at the horizontal middle plane in which the microchannel lies and Figure 5b shows the temperature distribution at the vertical middle plane along the width direction. Figure 6 shows the temperature distributions at the same middle planes with a larger channel width (200 $\mu$m) and the same materials. With different channel width, the temperature distributions are quite different because of the presence of Joule heating. As shown in Figure 5, the effect of

(37) Yousef, W. W.; Tarasuk, J. D.; McKenn, W. J. *J. Heat Tran.* **1982**, *104*, 493.

(38) Ren, L. Q.; Sinton, D.; Li, D. *J. Micromech. Microeng.* **2003**, *13*, 739.

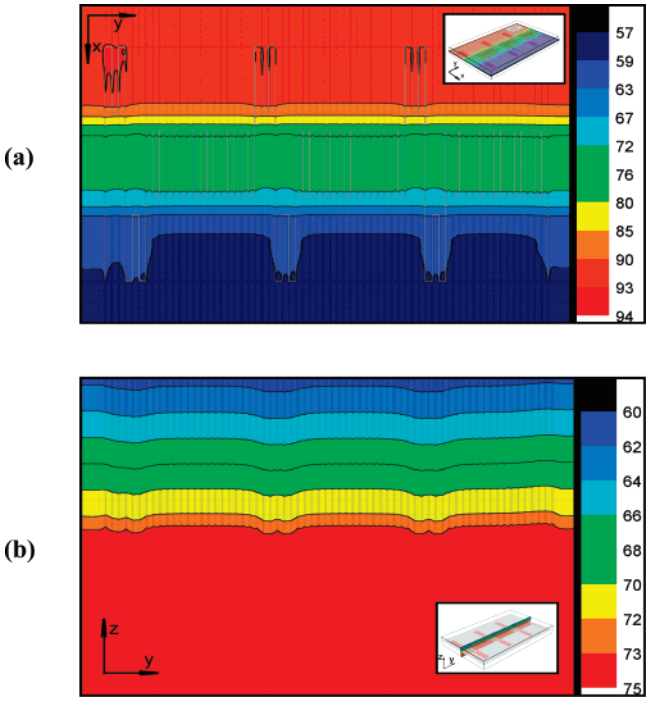


**Figure 5.** Temperature distribution of the chip at (a) the horizontal middle plane and (b) the vertical middle planes. The chip has a channel of 50 $\mu$m $\times$ 50 $\mu$m and is made of PDMS for the upper and glass for the lower layers. The applied electrical field strength is $E = 1.0 \times 10^4$ V/m.

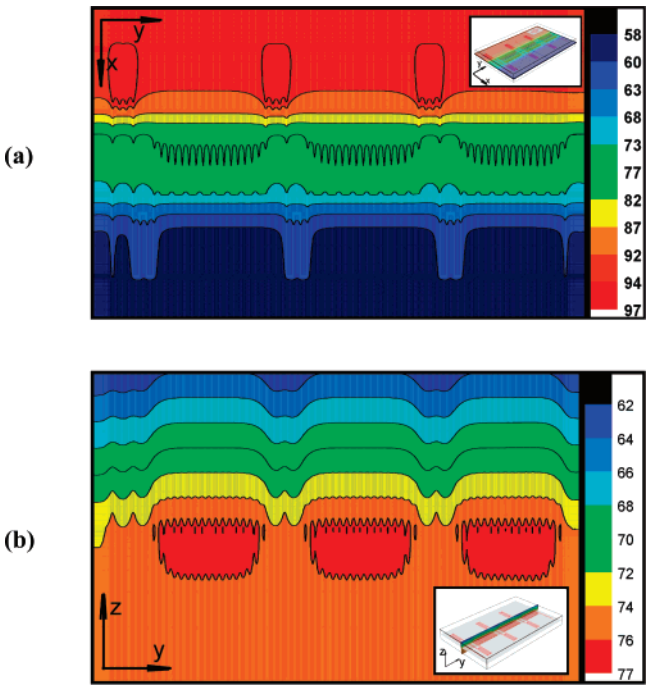


**Figure 6.** Temperature distribution of the chip at (a) the horizontal middle plane and (b) the vertical middle planes. The chip has a channel of 200 $\mu$m $\times$ 50 $\mu$m and is made of PDMS for the upper layer and glass for the lower layer. The applied electrical field strength is $E = 1.0 \times 10^4$ V/m.

Joule heating is very small when the channel is 50 $\mu$m $\times$ 50 $\mu$m. When the channel is larger (i.e., 200 $\mu$m $\times$ 50 $\mu$m in Figure 6), Joule heating increases the temperature of the fluid. As shown in Figure 6b, the temperature in the channel is even higher than the temperature at the bottom, which is kept constant. The reason why Joule heating in a larger channel is more appreciable than that in a smaller channel can be explained as follows. Smaller

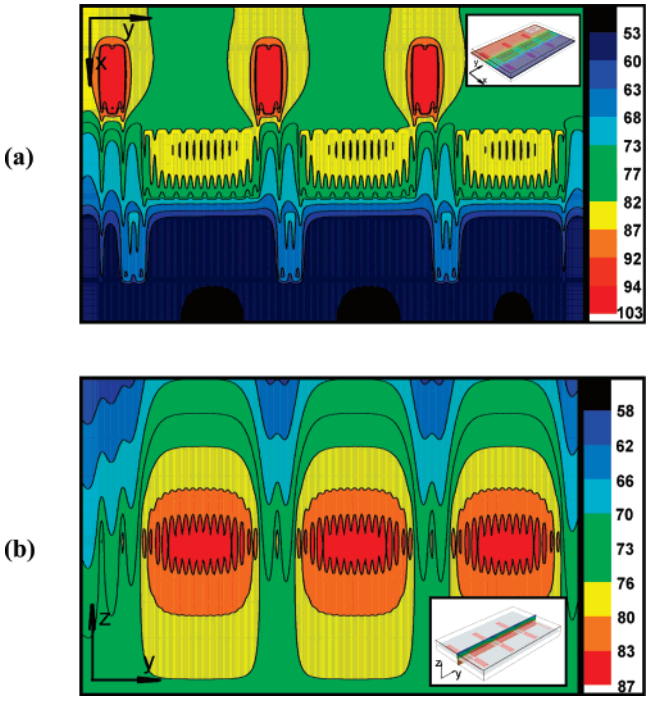


**Figure 7.** Temperature distribution of the chip at (a) the horizontal middle plane, and (b) the vertical middle planes. The chip has a channel of 200 $\mu$m $\times$ 50 $\mu$m and is made of PDMS for both the upper and lower layers. The applied electrical field strength is $E = 1.0 \times 10^4$ V/m.

channels have a large surface-to-volume ratio. The heat generated by Joule heating is directly proportional to the volume of channel for a given electrical field strength. The ability of dissipating heat is directly proportional to the area of the wall surface. So a large surface-to-volume ratio or, in other words, a smaller channel will surely bring about a stronger ability of dissipating Joule heating. Therefore, the temperature of the fluid is higher in a bigger channel size. Considering the effect of Joule heating, the temperature of the bottom should be designed a little lower than required if the channel size is big. For example, the temperature of the bottom should be designed about 2 °C lower than it should be, if the channel is 200 $\mu$m $\times$ 50 $\mu$m.

**4.2. Effect of Chip Material.** To see the influence brought by chip materials, two commonly used materials, PDMS and glass, were considered here. Figure 7 shows the temperature distributions for a PDMS chip. Compared to that shown in Figure 6, Joule heating is more evident when the entire chip is made of PDMS. The highest fluid temperature reaches 103 °C in Figure 7a, which is 6 °C higher than that in Figure 6a. This is because that the heat conductivity of PDMS (i.e., 0.15 $Wm^{-1}$ $K^{-1}$) is much lower than that of glass (i.e., 1.1 $Wm^{-1}$ $K^{-1}$) which leads to much slower heat dissipation. Thus, Joule heating accumulates near the microchannel and increases the temperature there up to 103 °C of maximum. From the pure thermal point of view, glass is more suitable for fabricating PCR chips because of its relatively high thermal conductivity. It makes controlling temperature much easier using glass as the chip material. But if well designed, the chip can also be fabricated using PDMS by properly decreasing the heating temperature at the bottom.

**4.3. Effect of Electrical Field Strength.** Joule heating is proportional to the square of the electrical field strength (i.e., $q = \sigma \vec{E}\vec{E}$). Figure 8 gives the temperature distribution of the chip when the electrical field strength (5000 V/m) is only half of the value used in Figure 6 and the microchannel is 200 $\mu$m $\times$ 50 $\mu$m. The lower layer is made of glass and the upper layer is made

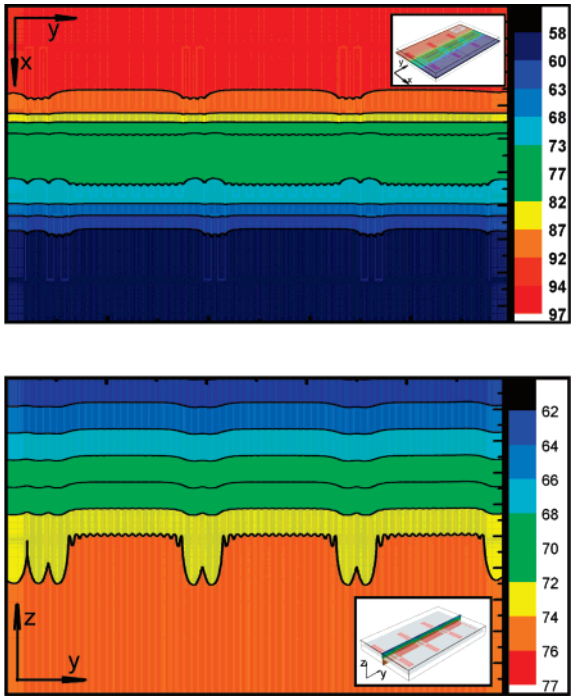


**Figure 8.** Temperature distribution of the chip at (a) the horizontal middle plane and (b) the vertical middle planes. The chip has a channel of 200 $\mu$m $\times$ 50 $\mu$m and is made of PDMS for both the upper and lower layers. The applied electrical field strength is $E = 0.5 \times 10^4$ V/m.

of PDMS. As shown in Figure 8, the effect of electrical field strength is very limited. Compared with Figure 6, Figure 8 indicates that the effect of Joule heating decreases sharply with the decrease of electrical field strength. Although decreasing the electrical field strength can reduce the effect of Joule heating, it increases the processing time for a continuous flow PCR chip, because of the decrease in fluid velocity.

## 5. Concluding Remarks

The presence of Joule heating in an electrokinteic-pumped continuous flow PCR chip makes the design and temperature control of the PCR chip much more difficult. Therefore, the effects of Joule heating on the temperature distribution in an electrokinteic-pumped continuous flow PCR chip were studied both analytically and numerically in this project. A 2D theoretical model was developed first and the analytical solution to this model was used to give a brief view of Joule heating effects for a continuous flow PCR chip. From the simplified theoretical model, an approximate solution was obtained (eq 11) showing the effects of the parameters, such as chip size, channel number, channel cross-sectional area and heat conductivity of the materials on the temperature distribution if Joule heating is considered. A 3D numerical model was developed to validate the analytical solution. Good agreement between numerically predicted temperature distribution and analytically predicted temperature distribution validated the developed analytical solution.

Parametric studies using the developed models show that (i) if the channel cross-sectional area is small, the effect of Joule heating is very limited because of its relatively high heat dissipation ability; (ii) glass is an ideal material for decreasing the effect of Joule heating; however, PDMS can also be used if the chip is well designed; (iii) the electrical field strength affects Joule heating greatly because Joule heating is proportional to the second power of the electrical field strength. Therefore, all the parameters such as chip size, channel dimensions, chip material and applied electrical field strength, should be optimized through numerical or analytical analysis prior to chip fabrication, which will shorten the iteration time among the design, fabrication and characterization of a microfluidic PCR chip.

**Acknowledgment.** The authors gratefully acknowledge the support of a Research Grant of the Natural Sciences and Engineering Research Council (NSERC) of Canada to C.L.R.

LA703201P